High-Power III–V/Si Integrated Wavelength Tunable Laser for L-Band Applications

Changpeng Li, Shaoshuai Sui, Feng Gao, Yiming Wang, Xiao Xu, and Jia Zhao

***Abstract*— We demonstrate a III-V/Si widely wavelength tunable laser covering the entire L-band for the optical communication systems. By carefully designing the silicon ring filter, low threshold current and high output power are expected. Using the standard silicon photonic process, the silicon filter chip is fabricated and compactly packaged with a reflective semiconductor optical amplifier. The low threshold current of 20 mA is achieved at 15 °C, and over 76 mW output power is obtained at 320 mA. The wavelength tuning range from 1565 nm to 1635 nm is realized with the side-mode suppression ratio larger than 50 dB. Furthermore, the intrinsic linewidth narrower than 25 kHz and relative intensity noise below −152 dB/Hz is achieved, which can support the coherent communications.**

***Index Terms*— Semiconductor lasers, tunable lasers, silicon photonics, hybrid integration, ring resonator.**

I. Introduction

TUNABLE lasers have attracted significant attention due to the extensive applications in optical communications [1], [2], [3], optical sensing [4], [5] and light detection and ranging (LIDAR) [6], [7]. Especially, in the coherent optical communications, the wide tuning range, large laser power and high spectral purity are required to meet the complex modulation formats and large transmission capacity [8]. In order to cope with the increasing bandwidth demand, the coherent optical communication system gradually extends to L-band, which requires a high-power and full L-band tunable laser. So far, several types of tunable semiconductor lasers have been presented, including the array of distributed feedback (DFB) lasers [9], [10], distributed Bragg reflector (DBR) lasers [11], [12] and external cavity lasers [13], [14], [15], [16], [17], [18]. Among them, the external cavity lasers have been widely studied and used because of the excellent laser linewidth and wavelength tuning range. Moreover, the external cavity based on silicon photonics technology can realize small footprint, high device integration and low cost, which has great potential in the tunable lasers.

However, electrically pumped tunable lasers on silicon-on-insulator (SOI) are most challenging due to the low light emission efficiency of silicon. In order to solve the problem, heterogeneous integration and hybrid integration are developed to realize high optical gain on silicon photonic platform [19], which provides a promising way to achieve high-efficiency silicon external-cavity tunable lasers. In recent years, many studies on tunable lasers have been reported using III-V/Si heterogeneous integration. In 2020, Tran et al. [14] reported a narrow-linewidth tunable laser based on a triple-ring mirror, and the linewidth below 220 Hz and tuning range from 1490 nm to 1600 nm are realized. In 2022, Morton et al. [15] demonstrated an integrated coherent tunable laser incorporating three ultra-low loss ring resonators, and a 118 nm wavelength tuning range is shown with Lorentzian linewidth < 100 Hz and maximum power of 15 mW. By adopting edge-coupling with high-performance III-V reflective semiconductor optical amplifier (RSOA), hybrid integration has been widely used in silicon external-cavity tunable lasers, which can simplify the laser fabrication process. In 2018, Guan et al. [16] demonstrated a III-V/silicon hybrid external cavity laser with a tuning range greater than 60 nm around the C-band, a maximum output power of 11 mW and a minimum linewidth of 37 kHz. In 2020, Fan et al. [17] proposed a silicon nitride-based hybrid laser with a tuning range of 70 nm and power of 23 mW, and an extremely narrow linewidth < 40 Hz is achieved. In the same year, Gao et al. [18] demonstrated a miniaturized hybrid tunable laser across the full C-band, and a record-high output power of 21.5 dBm has been achieved with a booster semiconductor optical amplifier.

In this paper, a high-power and widely tunable III-V/Si laser across L-band is demonstrated using an integrated silicon photonic wavelength filter as the external cavity. Through the hybrid integration technique, the compact laser is fabricated with the silicon photonic chip coupled to a broadband RSOA chip. By carefully designing the ring filter, low insertion loss and narrow filter bandwidth are achieved simultaneously. The laser shows a low threshold current of 20 mA and slope efficiency up to 0.25 W/A. The on-chip output power of 76 mW is observed at the continuous-wave (CW) injection of 320 mA. The wavelength tuning range of 70 nm is obtained across the entire L-band from 1565 nm to 1635 nm with a side-mode suppression ratio (SMSR) larger than 50 dB.

Manuscript received 11 January 2023; revised 5 June 2023 and 12 July 2023; accepted 18 September 2023. Date of publication 25 September 2023; date of current version 9 October 2023. This work was supported by the National Key Research and Development Program of China under Grant 2018YFA0209001. *(Corresponding author: Feng Gao.)*

Changpeng Li, Feng Gao, Yiming Wang, Xiao Xu, and Jia Zhao are with the School of Information Science and Engineering, Shandong University, Qingdao 266237, China (e-mail: lichangpeng@mail.sdu.edu.cn; gaofeng11@sdu.edu.cn; 202112667@mail.sdu.edu.cn; xuxiao@sdu.edu.cn; zhaojia@sdu.edu.cn).

Shaoshuai Sui is with Hisense Broadband Multimedia Technologies Company Ltd., Qingdao 266071, China (e-mail: suishaoshuai@hisense.com).

Color versions of one or more figures in this article are available at https://doi.org/10.1109/JQE.2023.3318589.

Digital Object Identifier 10.1109/JQE.2023.3318589

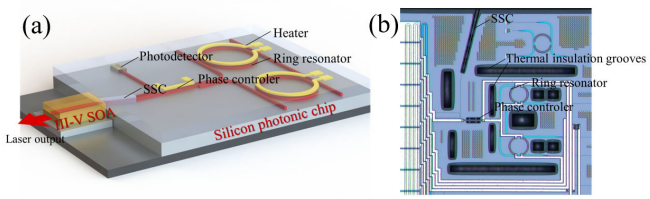

Fig. 1. (a) Schematic of the wavelength tunable laser. (b) Photograph of the silicon photonic external cavity chip.

In addition, the stability of the laser is experimentally studied with intrinsic linewidth below 25 kHz and relative intensity noise (RIN) below −152 dB/Hz.

II. Device Structure and Design

A. Structure of Laser

The schematic of the hybrid III-V/Si integrated external cavity laser is shown in Fig. 1(a). It is composed of a commercial InP/InGaAsP quantum well RSOA chip and a silicon photonic external cavity chip, which are edge-coupled using an active alignment technique. By monitoring the optical current of an on-chip Ge/Si photodiode, the optimal coupling position is obtained with the calculated coupling loss of 1.3 dB. The ROSA chip has a broadband spectrum with −2 dB bandwidth larger than 100 nm. It can support the saturation optical power beyond 80 mW with the front facet reflectivity of 6% to provide suitable optical feedback. The back facet of RSOA has a tilted waveguide to eliminate the effects of reflection on the laser, and the reflectivity of the back facet is lower than 0.01% coated with an anti-reflection (AR) film. The silicon photonic external cavity chip mainly includes a spot size converter (SSC), a multimode interference (MMI), a phase control section, a Vernier-ring filter and an integrated Ge/Si photodiode for power monitoring. The external cavity structure of loop configuration is chosen instead of series configuration to reduce the nonlinearity effects of the silicon ring resonators [20]. The SSC tapered down from a width of 500 nm to 120 nm is used, and a tilted 13.5° angle from the normal direction is designed to avoid back reflections and couple with RSOA chip. Wavelength selection is achieved by Vernier effect facilitated by two ring resonators with slightly different radius. TiN thermoelectric heaters with a thickness of 120 nm are fabricated on top of the ring resonators and phase control section to tune the laser wavelength via the thermo-optic effect. Thermal insulation grooves are set around the waveguide to cut off temperature crosstalk and improve heat tuning efficiency. The photograph of the silicon photonic chip is shown in Fig. 1(b).

B. Principle of Laser Design

The transmitted power spectrum of the drop port for one ring resonator can be expressed by

$$T_{drop1,2} = \left| \frac{k^2\sqrt{\alpha}\exp(-j\beta L_{1,2}/2)}{1-(1-k^2)\alpha\exp(-j\beta L_{1,2})} \right|^2 \quad (1)$$

where k is the electric-field coupling coefficients, α is the amplitude transmission, including both transmission loss and coupling loss, β is the effective propagation constant, and $L_{1,2}$ are the circumferences of the rings.

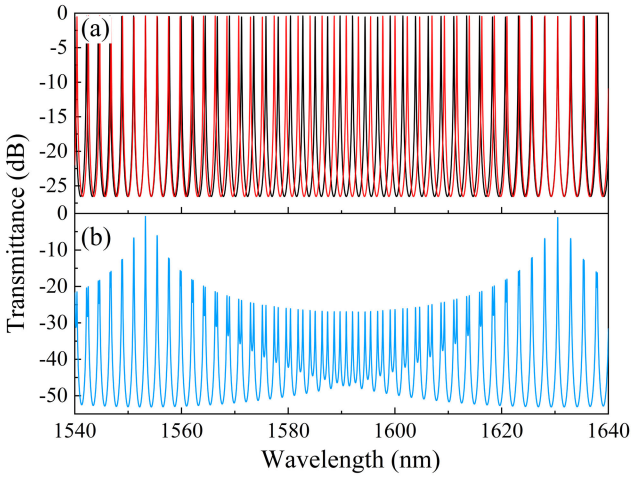

Fig. 2. (a) Normalized transmission spectra of two rings. (b) Synthesized spectrum of the double-ring resonator.

The total transmission spectrum for a double-ring resonator can be calculated as the product of the power transmittances of the two single rings, as shown in Fig. 2. Two rings with slightly different free spectral ranges (FSR) of 2.33 nm and 2.41 nm, respectively, are designed and used to extend the overall tuning range to 70 nm. By adjusting the power of heaters at the top of the ring resonators and phase control section, the waveguide refractive index can be changed, which leads to continuous tuning of wavelength.

The transmittance difference between the main and adjacent modes will greatly determine the capability of mode selection for the external cavity tunable lasers. A small modal gain difference will worsen the SMSR of the laser, which will potentially lead to multimode oscillation. In addition, multi-mode oscillation may also be caused by the large full-width at half maximum (FWHM) of the main mode. The modal gain difference and the main mode FWHM are dependent on the cross-coupling coefficient k, the amplitude transmission α and the circumference L. Although decreasing the coupling coefficient can easily achieve high modal gain difference and narrow FWHM, it will largely increase the insertion loss of the ring filter, consequently increase the laser threshold current and reduce the laser slope efficiency.

The laser linewidth property plays an important role in long-haul optical communications. For hybrid III-V/Si external cavity tunable lasers, the detailed spectral linewidth characteristics are analyzed and described by Henry's formula [21], [22] as follows:

$$\Delta v = \frac{\Delta v_0}{F^2} = \frac{\Delta v_0}{(1+A+B)^2} \quad (2)$$

$$\Delta v_0 = \frac{1}{4\pi}\frac{\hbar\omega_0 v_g^2 n_{sp}(\alpha_m+\alpha_{int})\alpha_m}{P_0\left[1+\frac{R_1}{|R_{eff}(\omega)|}\frac{1-|R_{eff}(\omega)|^2}{1-R_1^2}\right]}(1+\alpha_H^2) \quad (3)$$

$$A = \frac{1}{\tau_0}\mathrm{Re}\left\{j\frac{d}{d\omega}\ln R_{eff}(\omega)\right\} \quad (4)$$

$$B = \frac{\alpha_H}{\tau_0}\mathrm{Im}\left\{j\frac{d}{d\omega}\ln R_{eff}(\omega)\right\} \quad (5)$$

Here, Δv_0 is the Schawlow-Townes linewidth of the Fabry-Pérot laser with mirror reflectivity R_1 and R_{eff}, where R_{eff} represent the reflectivity of the effective mirror replacing the

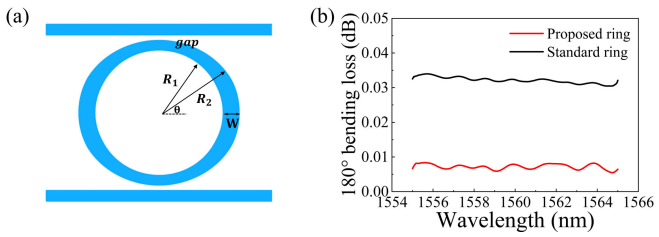

Fig. 3. (a) Schematic of design optimization of the ring resonator. (b) Measured 180° bending loss of the ring.

wavelength tunable filter [23]. n_{sp} is the population inversion factor, α_H is the linewidth enhancement factor, and P_0 is the output power. $\tau_0 = \frac{2n_g L_{active}}{c}$ is the photon round-trip time in the active section. α_m and α_{int} is the internal loss of the entire cavity and the active section respectively. Factor A reflects the increase in a roundtrip accumulated phase, and factor B represents the magnitude of the optical negative feedback effect.

From equations (2)-(5), we can derive two ways to compress the laser intrinsic linewidth. One way is to reduce the ring loss since the equivalent length of the weakly coupled ring can almost dominate the entire cavity length. Another way is to increase the equivalent cavity length by reducing the ring coupling coefficient [24], but it will conversely deteriorate the laser output power.

C. Design Optimization of Ring Resonators

According to the analysis in the previous section, we can conclude that realizing the low filter loss and small coupling coefficient simultaneously is beneficial to obtain high-performance silicon external cavity tunable lasers. Based on that, we carefully design and optimize the ring resonator, and the filter loss is largely reduced while keeping a small coupling coefficient. Figure 3(a) shows the top-view schematic diagram of the proposed ring resonator, and the ring is still near circular in shape. In the coupling region, the gap between the straight waveguide and the ring is 340 nm to obtain a low coupling coefficient, and the waveguide width of 500 nm is used to keep fundamental mode coupling. With the ring waveguide bending away from the coupling region, the ring radius (R_1) is gradually decreased from 100 μm to 43 μm. Then, via a short adiabatic taper, the waveguide is widened to 1 μm to significantly reduce the scattering loss caused by the roughness of the sidewalls, considering the propagating loss for the 1 μm wide waveguide is low to 0.17 dB/cm. By measuring cascaded bending structure, we experimentally obtain the half-ring loss of 0.033 dB and 0.008 dB for the standard and proposed ring resonator, respectively, as shown in Fig. 3(b).

Using the above measurement results, we theoretically investigate the properties of the double-ring filter as a function of the coupling coefficient by the transmission matrix method simulation. Figure 4(a) and (b) show the simulated curves of insertion loss and FWHM versus the field coupling coefficient. We can find that, for the standard design, a coupling coefficient larger than 0.45 with a corresponding FWHM of

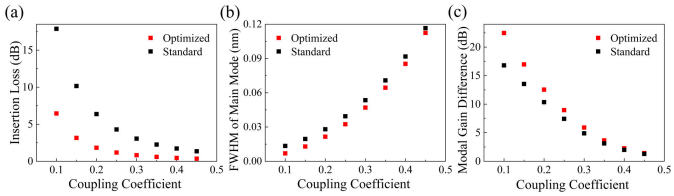

Fig. 4. Simulated (a) insertion loss, (b) FWHM of main mode, (c) modal gain difference of the double-ring filter as a function of the field coupling coefficient, for the optimized and standard rings.

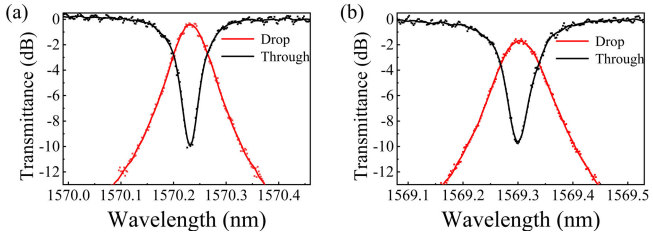

Fig. 5. Measured mode resonance of (a) optimized and (b) standard ring resonator.

0.116 nm is needed to achieve the insertion loss less than 1 dB. However, for the optimized design, the coupling coefficient can be reduced to 0.25 while keeping the insertion loss less than 1 dB and FWHM low to 0.033 nm. In addition, the modal gain difference of the double-ring filter is also calculated for both designed rings, as shown in Fig. 4(c). The modal gain difference is larger than 5 dB when the coupling coefficient is less than 0.3, which is enough to guarantee a high SMSR. Combining the loss and mode characteristics, we finally set the coupling coefficient around 0.28 to develop the high-performance tunable lasers.

With the optimized design, the single ring filter is fabricated corresponding to an FSR of 2.41 nm, and the filter curves are measured in Fig. 5(a). The insertion loss is 0.4 dB with a FWHM of 0.076 nm, and the corresponding Q-factor is up to 20600. As a contrast, the filter using a standard waveguide is also demonstrated with the same size, and Fig. 5(b) shows the measured filter curves. The insertion loss is up to 1.5 dB, and the FWHM is 0.085 nm. We can see that obvious improvement is achieved for the optimized ring resonator.

III. Laser Fabrication and Output Characteristics

A. Fabrication Process

The integrated silicon external cavity chips are fabricated on a SOI substrate with a 3 μm thick buried oxide layer and 220 nm thick top silicon layer, using standard CMOS-compatible silicon photonic process. The integrated chip has a width of 1 mm and a length of 1.6 mm. The RSOA chip with 1 mm length is mounted onto an aluminum nitride (AlN) base, and a thermistor close to the RSOA is bonded on the base to monitor the temperature. All the chips are affixed onto a temperature controller (TEC) to keep the specific operating temperature. In order to evaluate the laser optical spectra property, a single-mode polarization-maintaining fiber is fixed on the package via the isolator to couple the laser

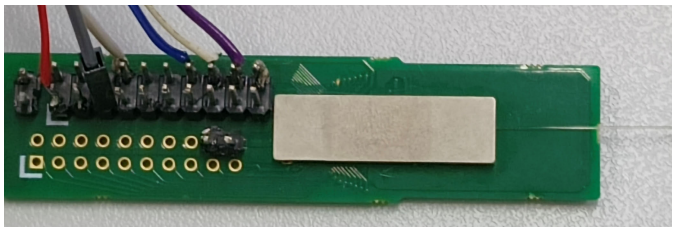

Fig. 6. Photograph of fabricated laser package assembly.

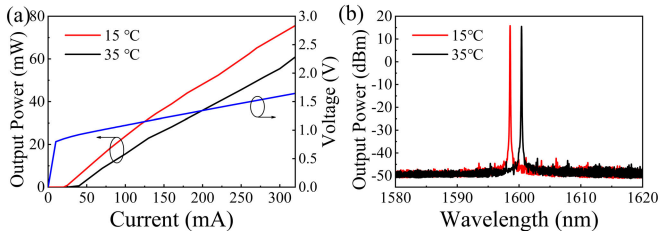

Fig. 7. (a) LIV curves and (b) Lasing spectra at 280 mA under TEC temperatures of 15 °C and 35 °C.

from the front facet of the RSOA chip, and the coupling loss of 1.4 dB is measured experimentally. The entire package assembly is placed on a small printed circuit board (PCB) to drive the tunable laser. Finally, a large metal lid is used to cover the assembly to provide protection. Figure 6 shows the microscope image of the fabricated tunable laser, and the assembly has a compact size with a length of 12 mm and a width of 4 mm contributed from the high device integration of the silicon filter chip.

B. Output Power and Lasing Spectrum

Figure 7(a) shows the measured LIV curves of the III-V/Si integrated wavelength tunable laser, and the output powers are measured under the different TEC control temperatures of 15 °C and 35 °C, respectively. The series resistance is 2.6 Ω, and the output power measured from the front facet of RSOA reaches 76 mW and 61 mW under the SOA injection current of 320 mA at 15 °C and 35 °C. The threshold current of 20 mA is achieved with slope efficiency up to 0.25 W/A at 15 °C, which benefits from the obvious improvement of ring resonators. By adjusting heaters on ring resonators and phase control section, the lasing spectra are measured using a high-precision optical spectrum analyzer (OSA) at an SOA current of 280 mA, as shown in Fig. 7(b). Excellent single-mode operation is realized with the SMSR larger than 55 dB. The stable single-mode lasing is realized as the RSOA injection current is up to 320 mA. With the current increasing further, the multimode operation and mode hopping are observed caused by the nonlinear effect in the ring resonator.

C. Wavelength Tuning and Noise Characteristics

By adjusting the heater power of one ring, superimposed spectra are obtained under an RSOA injection current of 180 mA, as shown in Fig. 8. Benefit from the broadband optical gain of RSOA and the slightly different FSRs of two rings, the wavelength tuning range of 70 nm is achieved from

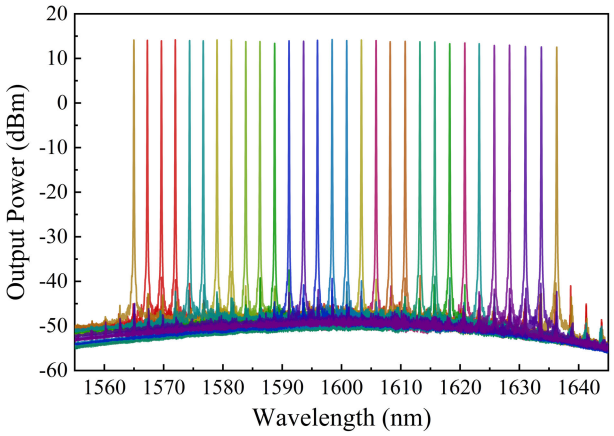

Fig. 8. Superimposed lasing spectra across a range of 70 nm measured by tuning one ring.

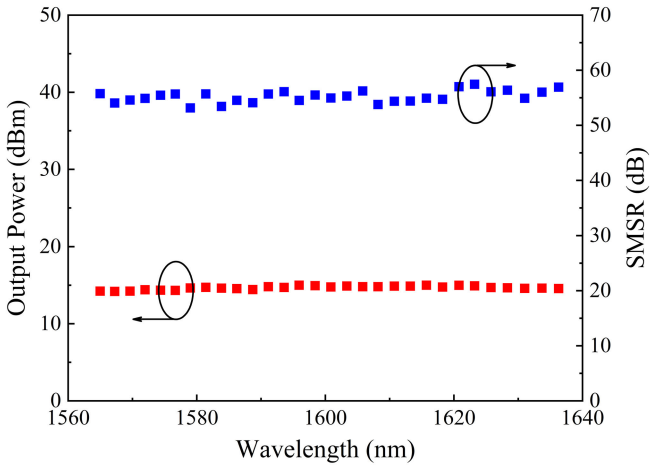

Fig. 9. Measured power and SMSR as a function of wavelength.

1565 nm to 1635 nm which can completely cover the L-band. Figure 9 shows the measurement results of the SMSR and output power versus the lasing wavelength. With the SMSR larger than 50 dB, stable single-mode operation is realized over the entire tuning range, which profits from the high modal gain difference of the optimized ring-resonators. Continuous wavelength tuning can also be achieved by simultaneously fine-tuning the heaters on two rings and phase control section, as shown in Fig. 10. The lasing wavelength shifts from 1598.48 nm to 1600.90 nm as the total power of two ring heaters increases from 32.58 mW to 168.48 mW. Therefore, the total power consumption of 135.9 mW is obtained to tune one FSR of 2.41 nm, and the continuous tuning efficiency of 0.018 nm/mW is calculated. The tuning efficiency up to 0.54 nm/mW is calculated. The tuning efficiency is significantly enhanced by etching more thermal insulation grooves close to the ring heaters. The total power consumption of the laser assembly is 1.3 W for covering the 70 nm wavelength tuning range, including the RSOA power consumption of 0.46 W with the injection current of 300 mA, the TEC power consumption of 0.7 W at the temperature of 35 °C and the heaters power consumption of 0.136 W.

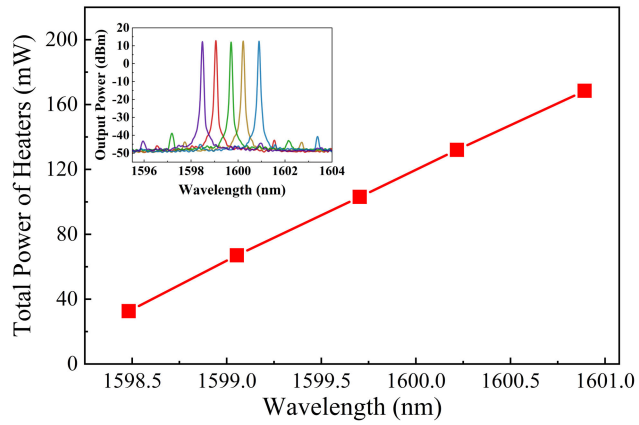

Fig. 10. Total thermal tuning power as a function of lasing wavelength. The inset shows the fine-tuned superimposed spectra.

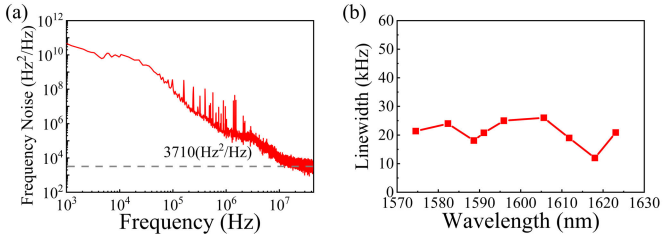

Fig. 11. (a) Typical frequency noise spectrum at 180 mA. (b) Measured linewidth as a function of wavelength.

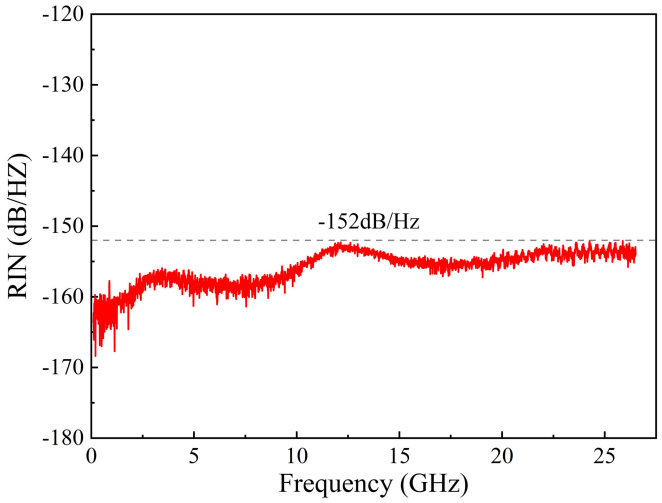

Fig. 12. Typical power spectrum of the RIN at 180 mA.

To further evaluate the performance in coherent optical communication, we experimentally measured the laser linewidth and RIN using SYCATUS A0040A optical noise analyzer and A0010A RIN testing system, respectively. Figure 11(a) shows a typical power spectral density (PSD) of frequency noise with lasing wavelength of 1620 nm and RSOA operating current of 180 mA. The intrinsic linewidth of the laser is calculated by using the PSD gradually flattening out in the frequency range of 20 to 40 MHz, avoiding the 1/f noise and other "technical noise" in the lower frequency range [25], [26]. We can find the white noise level is 3710 Hz^2/Hz, corresponding to the calculated intrinsic linewidth of 12 kHz. The intrinsic linewidth versus the lasing wavelength is also demonstrated in Fig. 11(b), and the intrinsic linewidth less than 25 kHz is realized across the entire tuning range. No significant degradation in the linewidth is observed as the injected current increases to 320 mA at 35 °C. Figure 12 shows the measured laser RIN curve at the RSOA current of 180 mA with the fiber-coupled output power of 31 mW. Via a variable optical attenuator, the optical power injected into an optical receiver is attenuated to 6 mW for RIN testing, and less than −152 dB/Hz is achieved.

IV. Conclusion

In summary, we have successfully demonstrated a high performance III-V/Si integrated wavelength tunable laser for L-band applications. By carefully optimizing the ring resonator, low insertion loss of 0.4 dB is realized with narrow FWHM less than 10 GHz. Through hybrid integration technique, the tunable laser is fabricated, and low threshold current of 20 mA is obtained at 15 °C, with output power of 76 mW at RSOA injection current of 320 mA. The widely wavelength tuning range of 70 nm is reported from 1565 to 1635 nm with SMSR larger than 50 dB. The intrinsic linewidth narrower than 25 kHz and RIN below −152 dB/Hz are achieved, which is suitable for digital coherent optical communication system.

References

[1] P. J. Winzer, A. H. Gnauck, C. R. Doerr, M. Magarini, and L. L. Buhl, "Spectrally efficient long-haul optical networking using 112-Gb/s polarization-multiplexed 16-QAM," *J. Lightw. Technol.*, vol. 28, no. 4, pp. 547–556, Feb. 15, 2010, doi: 10.1109/JLT.2009.2031922.

[2] H. Al-Taiy, N. Wenzel, S. Preußler, J. Klinger, and T. Schneider, "Ultra-narrow linewidth, stable and tunable laser source for optical communication systems and spectroscopy," *Opt. Lett.*, vol. 39, no. 20, pp. 5826–5829, Oct. 2014, doi: 10.1364/OL.39.005826.

[3] M.-H. Shih, K.-S. Hsu, K. Lee, K.-T. Lai, C.-T. Lin, and P.-T. Lee, "Compact tunable laser with InGaAsP photonic crystal nanorods for C-band communication," *IEEE J. Sel. Topics Quantum Electron.*, vol. 21, no. 6, Nov. 2015, Art. no. 4900505, doi: 10.1109/JSTQE.2015.2441959.

[4] L. He, Ş. K. Özdemir, J. Zhu, W. Kim, and L. Yang, "Detecting single viruses and nanoparticles using whispering gallery microlasers," *Nature Nanotechnol.*, vol. 6, no. 7, pp. 428–432, Jul. 2011, doi: 10.1038/NNANO.2011.99.

[5] R. Wang et al., "Widely tunable 2.3 μm III-V-on-silicon Vernier lasers for broadband spectroscopic sensing," *Photon. Res.*, vol. 6, no. 9, pp. 858–866, Sep. 2018, doi: 10.1364/PRJ.6.000858.

[6] W. Xie et al., "Heterogeneous silicon photonics sensing for autonomous cars," *Opt. Exp.*, vol. 27, no. 3, pp. 3642–3663, Feb. 2019, doi: 10.1364/OE.27.003642.

[7] Y. Zhu, S. Zeng, and L. Zhu, "Optical beam steering by using tunable, narrow-linewidth butt-coupled hybrid lasers in a silicon nitride photonics platform," *Photon. Res.*, vol. 8, no. 3, pp. 375–380, Mar. 2020, doi: 10.1364/PRJ.382852.

[8] N. Kobayashi et al., "Silicon photonic hybrid ring-filter external cavity wavelength tunable lasers," *J. Lightw. Technol.*, vol. 33, no. 6, pp. 1241–1246, Mar. 15, 2015, doi: 10.1109/JLT.2014.2385106.

[9] K. Tsuzuki et al., "Full C-band tunable DFB laser array copackaged with InP Mach–Zehnder modulator for DWDM optical communication systems," *IEEE J. Sel. Topics Quantum Electron.*, vol. 15, no. 3, pp. 521–527, May/Jun. 2009, doi: 10.1109/JSTQE.2009.2013972.

[10] R. Wang, S. Sprengel, G. Boehm, R. Baets, M.-C. Amann, and G. Roelkens, "Broad wavelength coverage 2.3 μm III-V-on-silicon DFB laser array," *Optica*, vol. 4, no. 8, pp. 972–975, Aug. 2017, doi: 10.1364/OPTICA.4.000972.

[11] G. Sarlet, G. Morthier, and R. Baets, "Wavelength and mode stabilization of widely tunable SG-DBR and SSG-DBR lasers," *IEEE Photon. Technol. Lett.*, vol. 11, no. 11, pp. 1351–1353, Nov. 1999, doi: 10.1109/68.803042.

[12] L. Yu et al., "Widely tunable narrow-linewidth lasers using self-injection DBR lasers," *IEEE Photon. Technol. Lett.*, vol. 27, no. 1, pp. 50–53, Jan. 1, 2015, doi: 10.1109/LPT.2014.2361833.
[13] R. M. Oldenbeuving, E. J. Klein, H. L. Offerhaus, C. J. Lee, H. Song, and K.-J. Boller, "25 kHz narrow spectral bandwidth of a wavelength tunable diode laser with a short waveguide-based external cavity," *Laser Phys. Lett.*, vol. 10, no. 1, Jan. 2013, Art. no. 015804, doi: 10.1088/1612-2011/10/1/015804.
[14] M. A. Tran, D. Huang, J. Guo, T. Komljenovic, P. A. Morton, and J. E. Bowers, "Ring-resonator based widely-tunable narrow-linewidth Si/InP integrated lasers," *IEEE J. Sel. Topics Quantum Electron.*, vol. 26, no. 2, Mar. 2020, Art. no. 1500514, doi: 10.1109/JSTQE.2019.2935274.
[15] P. A. Morton et al., "Integrated coherent tunable laser (ICTL) withultra-wideband wavelength tuning and sub-100 Hz Lorentzian linewidth," *J. Lightw. Technol.*, vol. 40, no. 6, pp. 1802–1809, Mar. 15, 2022, doi: 10.1109/JLT.2021.3127155.
[16] H. Guan et al., "Widely-tunable, narrow-linewidth III-V/silicon hybrid external-cavity laser for coherent communication," *Opt. Exp.*, vol. 26, no. 7, pp. 7920–7933, Apr. 2018, doi: 10.1364/OE.26.007920.
[17] Y. Fanet al., "Hybrid integrated InP-Si_3N_4 diode laser with a 40-Hz intrinsic linewidth," *Opt. Exp.*, vol. 28, no. 15, pp. 21713–21728, 2020, doi: 10.1364/OE.398906.
[18] Y. Gao et al., "High-power, narrow-linewidth, miniaturized silicon photonic tunable laser with accurate frequency control," *J. Lightw. Technol.*, vol. 38, no. 2, pp. 265–271, Jan. 15, 2020, doi: 10.1109/JLT.2019.2940589.
[19] M. Tang et al., "Integration of III-V lasers on Si for Si photonics," *Prog. Quantum Electron.*, vol. 66, pp. 1–18, Aug. 2019, doi: 10.1016/j.pquantelec.2019.05.002.
[20] T. Kita, R. Tang, and H. Yamada, "Narrow spectral linewidth silicon photonic wavelength tunable laser diode for digital coherent communication system," *IEEE J. Sel. Topics Quantum Electron.*, vol. 22, no. 6, Nov. 2016, Art. no. 1500612, doi: 10.1109/JSTQE.2016.2559418.
[21] R. Kazarinov and C. Henry, "The relation of line narrowing and chirp reduction resulting from the coupling of a semiconductor laser to passive resonator," *IEEE J. Quantum Electron.*, vol. QE-23, no. 9, pp. 1401–1409, Sep. 1987, doi: 10.1109/JQE.1987.1073531.
[22] C. Henry, "Theory of the linewidth of semiconductor lasers," *IEEE J. Quantum Electron.*, vol. QE-18, no. 2, pp. 259–264, Feb. 1982, doi: 10.1109/JQE.1982.1071522.
[23] L. A. Coldren, S. W. Corzine, and M. L. Masanovic, *Diode Lasers and Photonic Integrated Circuits*, 2nd ed. Hoboken, NJ, USA: Wiley, 2012.
[24] B. Liu, A. Shakouri, and J. E. Bowers, "Wide tunable double ring resonator coupled lasers," *IEEE Photon. Technol. Lett.*, vol. 14, no. 5, pp. 600–602, May 2002, doi: 10.1109/68.998697.
[25] M. A. Tran, D. Huang, and J. E. Bowers, "Tutorial on narrow linewidth tunable semiconductor lasers using Si/III-V heterogeneous integration," *APL Photon.*, vol. 4, no. 11, Nov. 2019, Art. no. 111101, doi: 10.1063/1.5124254.
[26] C. Luo, R. Zhang, B. Qiu, and W. Wang, "Waveguide external cavity narrow linewidth semiconductor lasers," *J. Semicond.*, vol. 42, no. 4, Apr. 2021, Art. no. 041308, doi: 10.1088/1674-4926/42/4/041308.

Changpeng Li received the B.S. degree from Shandong University, Jinan, Shandong, China, in 2018. He is currently pursuing the Ph.D. degree with the School of Information Science and Engineering, Shandong University, Qingdao. His current research interests include silicon photonics and semiconductor laser diodes.

Shaoshuai Sui received the Ph.D. degree in physics from the Institute of Semiconductors, Chinese Academy of Sciences, Beijing, China, in 2016. He is currently with Hisense Broadband Multimedia Technologies Company Ltd., Qingdao, Shandong, China, and focused on the III–V/SOI hybrid integration and silicon photonic integrated circuits.

Feng Gao received the Ph.D. degree in physical electronics from the Institute of Semiconductors, Chinese Academy of Sciences, Beijing, China, in 2016. She was with Hisense Broadband Multimedia Technologies Company Ltd., Qingdao, Shandong, China, where she worked on design and simulation of the high-speed DFB lasers from 2016 to 2021. She joined the School of Information Science and Engineering, Shandong University, Qingdao, in 2021, as an Associate Professor. Her research interests include semiconductor optoelectronic materials, devices, and photonic integrated circuits.

Yiming Wang received the B.S. degree from the Qingdao University of Technology, Qingdao, Shandong, China, in 2021. He is currently pursuing the Ph.D. degree with the School of Information Science and Engineering, Shandong University, Qingdao. His current research focuses on high-speed germanium-silicon photodetector and reliability of integrated optoelectronics devices.

Xiao Xu received the B.S. degree from the University of Electronic Science and Technology of China, Chengdu, China, in 2014, and the Ph.D. degree from Shanghai Jiao Tong University, Shanghai, China, in 2019. She is currently an Associate Professor with the School of Information Science and Engineering, Shandong University, Qingdao, Shandong. Her major research interests include optical interconnects and optical waveguide devices.

Jia Zhao received the B.S. and Ph.D. degrees from Shandong University, Jinan, Shandong, China, in 2006 and 2011, respectively. He is currently working as a Professor with the School of Information Science and Engineering, Shandong University, Qingdao. His research interests include nanophotonic, chip-scale optical interconnection, and computational electromagnetics.